Aerodynamic control capability of a wing-flap in hypersonic, rarefied regime

Gennaro Zuppardi[*]

*Department of Industrial Engineering, University of Naples "Federico II",
Piazzale Tecchio 80, 80125 Naples, Italy*

Abstract.   The attitude aerodynamic control is an important subject in the design of an aerospace plane. Usually, at high altitudes, this control is fulfilled by thrusters so that the implementation of an aerodynamic control of the vehicle has the advantage of reducing the amount of thrusters fuel to be loaded on board. In the present paper, the efficiency of a wing-flap has been evaluated considering a NACA 0010 airfoil with a trailing edge flap of length equal to 35% of the chord. Computational tests have been carried out in hypersonic, rarefied flow by a direct simulation Monte Carlo code at the altitudes of 65 and 85 km, in the range of angle of attack 0-40 deg. and with flap deflection equal to 0, 15 and 30 deg.. Effects of the flap deflection have been quantified by the variations of the aerodynamic force and of the longitudinal moment. The shock wave-boundary layer interaction and the shock wave-shock wave interaction have been also considered. A possible interaction of the leading edge shock wave and of the shock wave arising from the vertex of the convex corner, produced on the lower surface of the airfoil when the flap is deflected, generates a shock wave whose intensity is stronger than those of the two interacting shock waves. This produces a consistent increment of pressure and heat flux on the lower surface of the flap, where a thermal protection system is required.

Keywords: hypersonic; rarefied Aerodynamics; effects of wing-flap deflection; shock wave-boundary layer interaction; shock wave-shock wave interaction; direct simulation Monte Carlo method

1. Introduction

The presence in the scientific, aerospace panorama of projects of forthcoming winged aerospace planes as per the European Phoebus (Tausche *et al.* 2009), Skylon (Varvill and Bond 2011) and SpaceLiner (Sippel *et al.* 2011) and the American Boeing X51A waverider, Boeing X37B and many others, flying through Atmosphere at very high velocity and crossing all rarefaction regimes, from free molecular flow to continuum, stimulates the study of Aerodynamics of lifting bodies in hypersonic, rarefied regime. One of the most interesting aspects of the design of an aerospace plane is the attitude control. The attitude control of an aerospace plane is fulfilled by thrusters at high altitudes and by aerodynamic surfaces (wing-flaps, body-flaps, elevons and so on) at low altitudes. Combining thrusters with aerodynamic control of a vehicle also at high

---

∗Corresponding author, Lecturer, E-mail: zuppardi@unina.it

altitude provides the undoubted advantage of reducing the amount of fuel for the thrusters to be loaded on the vehicle.

The present paper is the follow-on of two former articles by the present author (Zuppardi *et al.* 2011), (Zuppardi *et al.* 2014) where the effect of the wing trailing edge flap was evaluated on the flight performances of the FTB-X and SpaceLiner-7.1 aerospace-planes, respectively. More specifically, Zuppardi and co-workers verified, for FTB-X, that the altitude at which an aerodynamic control begins to be significant during the re-entry, is about 70 km and evaluated the effects of the flap deflection on the aerodynamic coefficients of the SpaceLiner-7.1 vehicle in the altitude range 100-250 km. More specifically, Zuppardi verified the capability of an aerodynamic control in hypersonic rarefied flow field and therefore the possibility to trim the vehicle by wing-flaps during the high altitude re-entry path.

The basic analysis of an aerodynamic attitude control relies on the study of the aerodynamic behavior of a wing section in clean (or with no flap deflection) and flapped configurations. In the present paper, a computational analysis has been carried out on the NACA-0010 airfoil at the altitudes of 65 and 85 km, in the range of angle of attack 0-40 deg. and flap deflection of 15 and 30 deg. in hypersonic, continuum low density regime. The investigated problem is essentially of academic interest; it is obvious that configurations of real aerospace planes are much more complex. On the other hand, the main aim of the present work is to highlight the capability of a wing flap to change the aerodynamic forces and moments. Real applications for the aerodynamic trim and vehicle control, based on the equilibrium of forces and moments around the center of gravity, are outside the scope of the present paper.

Computer tests have been carried out by a direct simulation Monte Carlo (DSMC) code. As well known, the DSMC method (Bird 1998), (Shen 2005) provides the solution of a flow field in rarefied regime. It overcomes the failure of the Computational Fluid-Dynamic (CFD) procedure due to the failure, in rarefied flow, of the phenomenological equations of Newton, Fourier and Fick. In addition, for the present application, using a DSMC code is mandatory. Indeed, the complexity of the flow field, due to shock wave/boundary layer interaction, linked to the compression ramp produced by the flap deflection and the interaction of the shock wave, produced by the airfoil leading edge, could make difficult to solve the flow field by CFD.

The aerodynamic parameters of interest for this analysis are the global aerodynamic force and the longitudinal moment coefficients, the aerodynamic efficiency and quantities providing local aerodynamic and thermal loads, such as pressure and heat flux, along the airfoil lower surface. The cross effects of the angle of attack and of the deflection angle of the flap are evaluated on the global aerodynamic coefficients. Furthermore, the effects of the shock wave-boundary layer and of the shock wave-shock wave interferences are evaluated on the pressure and heat flux distributions.

2. Shock wave-boundary layer and shock wave-shock wave interactions

The aerodynamic problem here studied involves two "classical" interactions: Shock Wave-Boundary Layer Interaction (SWBLI), Shock Wave-Shock Wave Interaction (SWSWI). SWBLI is related to a ramp, such as that produced by the lower surface of its deflected flap. This problem was studied by Delery and Panaras (1996), Delery and Marvin (1986) and summarized by Bertin (1994). SWSWI is related to the interaction of two weak shock waves of the same family. In the present study a shock wave is produced by the airfoil leading edge, the other one is produced by the ramp. This type of interaction was studied by Edney (1968), reported by Korkegi (1971) and
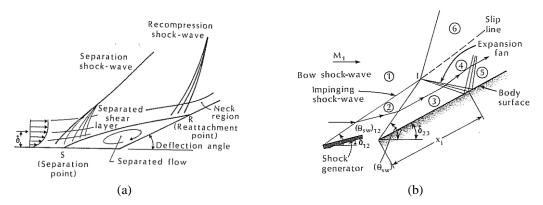
Fig. 1 (a) Sketch of the shock wave-boundary layer interaction on a concave corner and (b) of the shock wave-shock wave interaction (from Bertin 1994)

summarized by Bertin (1994), is labelled in the international literature as Type VI interaction.

The flap deflection generates a concave wedge (or a ramp) on the airfoil lower surface, producing an adverse pressure gradient. This pressure disturbance propagates upstream in the subsonic region of the boundary layer and produces a thickening of the boundary layer which separates forming a separation bubble (Fig. 1(a)); points "S" and "R" identify the separation and the reattachment points, respectively. A complex "lambda" shock wave system is generated. This system is made of a "separation" shock wave at the beginning of the bubble (or separation point) and a "recompression" shock wave at the reattachment point. Both shock waves are produced by the coalescence of compression Mach waves and are of the same family but of different slopes, thus they can merge at some distance from the corner. The point where the shock waves meet is identified as "triple point" (not shown in figure). A number of measurements, reported by Delery and Panaras (1996) and by Delery and Marvin (1986) verified that the main parameters, influencing SWBLI, therefore the extension of the separation bubble or of the "dead air" region in contact with the wall are: 1) upstream Mach number, 2) Reynolds number, 3) wedge angle, 4) thickness of the incoming boundary layer, 5) wall temperature, 6) chemical state of the gas. The intensity of SWBLI increases with the wedge angle, the Reynolds number, the wall temperature and decreases with the Mach number.

Type VI of SWSWI occurs when two weak shock waves of the same family intersect; the intersection point is identified in Fig. 1(b) as point I. The two interacting shock waves form a single weak shock wave outboard the intersection and a slip line originates from point I. This slip line separates the flow field in two regions: 1) where the flow passes through two shock waves (region 4), 2) where the flow passes through a single shock wave (region 6). Thus pressure should be higher in 4 than in 6. For decreasing pressure in 4, and therefore for restoring the equilibrium of the slip line, an expansion fan generates from point I. This fan impinges onto the body surface, producing a decrease of pressure and heat flux.

3. Direct simulation Monte Carlo method and DS2V code

The DSMC method (Bird 1998, Shen 2005) considers the gas as made up of molecules and relies on the kinetic theory of the gases. The method computes the evolution of millions of

simulated molecules, each one representing a large number (say 10^{13}-10^{14}) of real molecules in the physical space. Intermolecular and molecule-surface collisions are evaluated. The computational domain is divided in cells that are used for selecting the colliding molecules and for sampling the macroscopic, fluid-dynamic quantities. The method does not suffer from numerical instabilities but is inherently unsteady with a steady solution achievable after a sufficiently long simulation time.

The DSMC code, used in the present work, is DS2V-64bits (Bird 2012), specific for 2D/Axis-symmetric flow fields. In this code, air is modelled as a gas made of five neutral reacting species (O_2, N_2, O, N and NO). The code relies on the built-in Gupta-Yos-Thompson (Gupta *et al.* 1989) chemical model, consisting of 23 forward/reverse chemical reactions. The code is "sophisticated". As widely reported in literature (Bird 2006, Bird *et al.* 2009, Gallis *et al.* 2009), a sophisticated DSMC code implements computing procedures which guarantee a higher efficiency and accuracy with respect to the "basic" DSMC codes. In fact, a sophisticated code relies on two sets of cells (collision and sampling cells) with the related cell adaptation and implements methods promoting nearest neighbour collisions. This type of code generates automatically computational parameters such as numbers of cells and of simulated molecules by the input numbers of megabytes and of free stream number density. It uses a radial weighting factor in solving axial-symmetric flow fields and provides optimal time step. Finally, the same collision pair cannot have sequential collisions.

Besides being sophisticated, DS2V is also advanced because it allows the user to evaluate the quality of a simulation. The user, in fact, can verify that the number of simulated molecules and collision cells are adequate by means of the on line visualization of the ratio between the molecule mean collision separation (mcs) and the mean free path (λ) in each collision cell. In addition, the code allows the user to change (or to increase) the number of simulated molecules during the run. The ratio mcs/λ has to be less than unity everywhere in the computational domain; Bird (2006) suggests 0.2 as a limit value for an optimal quality of the run. In addition, the code provides information about the stabilization of the runs by means of the profile of the number of simulated molecules as a function of the simulated time. The stabilization of a DSMC calculation is achieved when this profile becomes jagged and included within a band defined by the standard deviation of the number of simulated molecules.

4. Test conditions and quality of the runs

Computer tests have been carried out on the "classic" NACA 0010 airfoil in clean and flapped configurations. Figs. 2(a), (b), (c) show the airfoil geometries with three flap angles (δ): δ=0, 15, 30 deg., respectively. The chord (c) was 2 m and the flap hinge was located at 65% of the chord (x=1.30 m) or at the curvilinear abscissa (s) from the leading edge: s=1.48 m. The airfoil surface was approximated by 1000 flat panels (500 on the lower surface and 500 on the upper surface). The wall was assumed non-catalytic and at uniform temperature of 300 K. The 2-D computing domain was a rectangle: L_x=2.5 m, L_y=1.1 m.

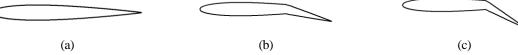   (a)   (b)   (c)
Fig. 2 NACA0010 airfoil with (a) δ=0 deg., (b) 15 deg., and (c) δ=30 deg.

Table 1 Free stream parameters

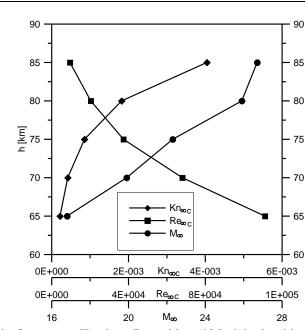| h [km]	T_∞ [K]	ρ_∞ [kg/m^3]	N_∞ [m^{-3}]	V_∞ [m/s]	M_∞	$Re_{\infty c}$	$Kn_{\infty c}$
85	189	8.22×10^{-6}	1.71×10^{20}	7355	26.7	9500	4.0×10^{-3}
80	199	1.85×10^{-5}	3.84×10^{20}	7321	25.9	20333	1.8×10^{-3}
75	208	3.99×10^{-5}	8.30×10^{20}	6476	22.3	37375	8.5×10^{-4}
70	220	8.28×10^{-5}	1.72×10^{21}	5933	19.9	68032	4.2×10^{-4}
65	233	1.63×10^{-4}	3.39×10^{21}	5163	16.8	111065	2.1×10^{-4}

Fig. 3 Profiles of the free stream Knudsen, Reynolds and Mach in the altitude interval 65-85 km

Table 1 reports some free stream aerodynamic parameters: velocity (V_∞) was evaluated at different altitudes along a typical re-entry trajectory of the FTB-X vehicle (Zuppardi 2011), temperature (T_∞), density (ρ_∞) and number density (N_∞) were provided by the U.S. Standard Atmosphere 1976. Air composition was standard or, in terms of molar fractions (α), α_{N2}=0.79 for Nitrogen and α_{O2}=0.21 for Oxygen.

Fig. 3 shows the profiles of the Mach (M_∞), Reynolds (Re_∞) and Knudsen ($Kn_{\infty c}$) numbers, both based on the airfoil chord, in the altitude (h) interval 65-85 km. The Knudsen number verifies that in this altitude interval, the flow field is in continuum low density regime. In fact, according to Moss (1995), the transitional regime is defined by: $10^{-3}<Kn_{\infty c}<50$.

The DS2V runs were carried out at the altitudes of 65 and 85 km and at the angles of attack (α) ranging from 0 to 40 deg., with an interval of 5 deg., and considering three flap deflections: δ=0, 15, 30 deg.; the total number of runs was 54. An extra run at the most severe conditions for the DSMC method (i.e.,: h=65 km, α=40 deg., δ=30 deg.) was made to evaluate the surface catalytic effect. The considered surface reactions were: O+O$\rightarrow$O$_2$, N+N$\rightarrow$N$_2$, N+O$\rightarrow$NO.

All runs satisfied the requirements of a good quality in terms of DSMC and fluid-dynamic criteria. For example, Table 2 reports some run parameters at h=65 km and α=40 deg. and for the three flap angles.

Table 2 DS2V run parameters at h=65 km and α=40 deg.

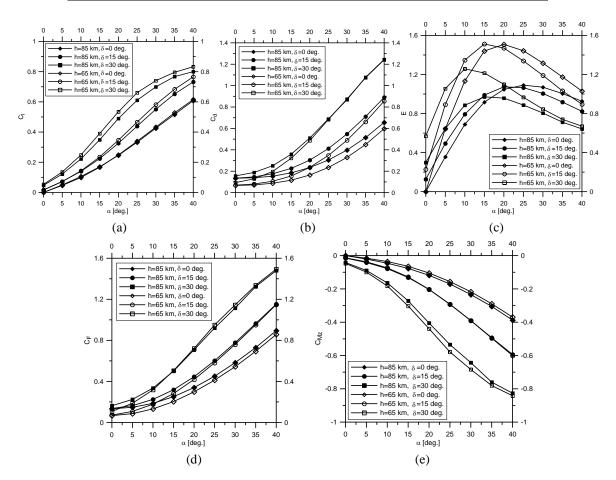| δ [deg.]	N_m	N_c	N_s	mcs/mfp	t_s/t_f
0	4.9×10^7	3.5×10^6	8.5×10^4	0.35	3.5
15	5.3×10^7	1.9×10^6	8.5×10^4	0.50	3.5
30	6.7×10^7	1.5×10^6	7.9×10^4	0.85	3.5

Fig. 4 Profiles of (a) lift and (b) drag coefficients, (c) aerodynamic efficiency, (d) aerodynamic force and (e) longitudinal moment coefficients as functions of the angle of attach

The parameters are the numbers of simulated molecules (N_m), of collision cells (N_c), of sampling cells (N_s), the ratio mcs/mfp and the ratio of the simulation time (t_s) to the time (t_f) required to travel a distance equal to the airfoil chord at the free stream velocity. During the runs, the stabilization of the DSMC computations can be verified by the profile of the "molecule number history"; a DSMC computation is stabilized when this profile gets jagged. Even though the values of mcs/λ do not satisfy the optimal limit value of 0.2, they have been smaller than one in each run. Furthermore, the ratio t_s/t_f, for each run, satisfies reasonably the criterion for the stabilization from a fluid-dynamic point of view.

5. Analysis of the results

5.1 Force and moment coefficients

Figs. 4(a) to 4(e) show the profiles of lift coefficient (C_l, (a)), drag coefficient (C_d, (b)), aerodynamic efficiency ($E=C_l/C_d$, (c)), aerodynamic force coefficient ($C_F = \sqrt{C_l^2 + C_d^2}$, (d)), longitudinal moment coefficient (C_{Mz}, (e), as functions of the angle of attack. Each chart includes the results corresponding to the clean configuration ($\delta=0$) and to the cases $\delta=15$, 30 deg., at the altitudes $h=65$ and 85 km. The pole of the longitudinal moment is the airfoil leading edge. The results show that the influence of the altitude (and therefore of the Knudsen, Reynolds and Mach numbers, see Table 1) is not very relevant. However the influence on C_l and C_d, even though small, is amplified on the aerodynamic efficiency and, as expected, E decreases with rarefaction or altitude. On the opposite, the flap deflection produces strong effects even at high altitudes.

Tables 3 and 4 report the percentage variations of these parameters with respect to the same values in clean configuration for each angle of attach and for the two flap deflections ($\delta=15$, 30 deg.). At the two altitudes and flap deflections, due to the cross effects of the angles of attack and of the flap deflection, the percentage variations (or increments) of the lift and of the moment coefficients decrease with the angle of attack. Vice versa, the drag coefficient increases. For this reason, the following analysis will be focused on the aerodynamic force and on the longitudinal moment coefficients.

At $h=65$ km and $\delta=30$ deg., the highest percentage increments occur at the angles of attack equal to 15 deg. for C_F (149%) and to 5 deg. for C_{Mz} (531%). At $h=85$ km and $\delta=30$ deg., the highest percentage increments are found at the angles of attack of 20 deg. for C_F (108%) and 5 deg. for C_{Mz} (331%).

Table 3 Percentage variations of the lift, drag, aerodynamic force and longitudinal moment: $h=65$ km

$\alpha°$	C_l, $\delta=15°$	C_d, $\delta=15°$	C_F, $\delta=15°$	C_{Mz}, $\delta=15°$	C_l, $\delta=30°$	C_d, $\delta=30°$	C_F, $\delta=30°$	C_{Mz}, $\delta=30°$
0	==	5	8	==	==	41	62	==
5	54	12	26	138	192	79	119	531
10	44	22	35	108	151	126	141	413
15	41	34	39	99	134	177	149	370
20	40	43	41	94	115	195	142	320
25	37	48	41	88	95	191	131	271
30	35	49	40	80	71	166	111	215
35	29	47	37	72	51	139	93	170
40	24	43	34	63	35	108	74	128

Table 4 Percentage variations of the lift, drag, aerodynamic force and longitudinal moment: $h=85$ km

$\alpha°$	C_l, $\delta=15°$	C_d, $\delta=15°$	C_F, $\delta=15°$	C_{Mz}, $\delta=15°$	C_l, $\delta=30°$	C_d, $\delta=30°$	C_F, $\delta=30°$	C_{Mz}, $\delta=30°$
0	==	1	2	==	==	17	22	==
5	46	6	11	100	146	36	52	331
10	32	15	21	71	110	64	80	257
15	32	22	27	71	106	94	99	253
20	33	29	31	72	99	118	108	242
25	32	35	34	71	84	126	104	213
30	30	38	33	67	64	118	91	175
35	26	38	32	62	48	110	81	149
40	21	36	29	53	32	90	65	113

Table 5 Aerodynamic efficiency (E): *h*=65 km

$\alpha°$	$\delta=0°$	$\delta=15°$	$\delta=30°$
0	0	0.13	0.30
5	0.36	0.49	0.65
10	0.69	0.79	0.89
15	0.92	0.99	0.97
20	1.05	1.07	0.96
25	1.09	1.07	0.89
30	1.07	1.01	0.81
35	1.00	0.92	0.71
40	0.93	0.82	0.64

Table 6 Aerodynamic efficiency (E): *h*=85 km

$\alpha°$	$\delta=0°$	$\delta=15°$	$\delta=30°$
0	0	0.23	0.57
5	0.64	0.89	1.06
10	1.13	1.35	1.26
15	1.44	1.51	1.22
20	1.51	1.47	1.10
25	1.44	1.34	0.97
30	1.32	1.19	0.85
35	1.17	1.03	0.74
40	1.03	0.90	0.67

Tables 5 and 6 report the values of the aerodynamic efficiency at the two altitudes. The maximum efficiency angle of attack is of interest for an aerospace plane since it is the most probable re-entry angle. The maximum efficiency angle of attack varies from 20 to 10 deg. at *h*=65 km and from 15 to 25 deg. at *h*=85 km, in both cases with δ changing from 0 to 30 deg.. These values are comparable with those computed for the SpaceLiner (Zuppardi *et al.* 2014). For example, at *h*=100 km ($M_\infty \cong 12$, $Kn_{\infty L} \cong 2.16 \times 10^{-3}$, $Re_{\infty L} \cong 8.04 \times 10^3$, fuselage length *L*=63 m), the maximum aerodynamic efficiency is 1.04 and the corresponding angle is 15 deg. These angles are also meaningful because intermediate between those corresponding to the maximum variations of the aerodynamic force and longitudinal moment. Indeed ($\Delta C_F/C_F\%$) and ($\Delta C_{Mz}/C_{Mz}\%$) are maximum for α=15 and α=5 deg. at *h*=65 km and α=20, α=5 deg. at h=85 km, respectively.

5.2 SWBLI and SWSWI effects

As already mentioned in sect. 2, both SWBLI and SWSWI related to the flap deflection, can produce strong increments of aerodynamic (pressure) and thermal (heat flux) loads along the airfoil lower surface. Figs. 5(a) and 5(b) show the pressure (a) and heat flux (b) profiles along the airfoil lower surface as functions of the curvilinear abscissa, at α=10 and 15 deg., δ=0 and 30 deg., *h*=65 and 85 km. Both figures show profiles correctly decreasing from leading edge to flap hinge. Due to the shock wave, departing from the position of the hinge, both pressure and heat flux start to increase. In these conditions, both profiles are not able to clearly define a separation bubble. The
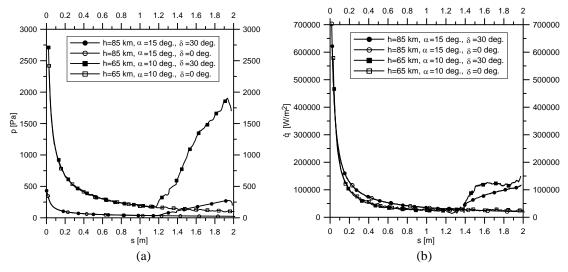
Fig. 5 Profiles of pressure (a) and heat flux (b) along the airfoil lower surface

Table 7 Interaction parameters: δ=30 deg.

h [km]	$\dot{q}_{max}/\dot{q}_{LE}$	$\dot{q}_{max}/\dot{q}_{\delta=0}$	p_{max}/p_{LE}	$p_{max}/p_{\delta=0}$
65	0.1	6.0	0.5	18.5
85	0.1	5.9	0.6	11.0

subsequent decrease up to the trailing edge is due to the presence of expansion Mach waves in the shock layer. At these angles of attack, the intensity of the shock wave is not very high and the subsequent extension of the expansion waves involves only a very small part of the flap surface (see Fig. 5(a)). Table 7 provides an evaluation of the increments of these quantities, measured by the ratios of the maximum values p_{max} and $\dot{q}_{max}$ at the maximum efficiency angles of attack (i.e., α_{Emax}=10 deg. at h=65 km and α_{Emax}=15 deg. at h=85 km) and the related values at the leading edge with respect to those computed at the same positions in clean configuration. At low angles of attack, the increments of both heat flux and pressure are much lower than the respective values at the leading edge, while they are more consistent on the flap.

The pressure and the heat flux profiles along the airfoil lower surface, computed at the most severe test conditions (h=65 km, α=40 deg., δ=30 deg.) are shown in Figs. 6(a) and 6(b) with the amplified SWBLI and the SWSWI effects. Both pressure and heat flux profiles show two relative maxima, the first one linked to the shock wave coming from the hinge, the much higher second one, linked to the interaction of the shock waves. The figures show for comparison also the profiles of the same quantities computed with δ=0 and δ=15 deg.. In order to quantify the increments of pressure and of heat flux on the flap surface, Table 8 reports the ratios of the maximum values of pressure and of heat flux at δ=30 deg., 15 deg. and the same values at the leading edge and with δ=0 deg. at the same position. At δ=30 deg., both heat flux and pressure get values comparable with those at the leading edge and are even one order of magnitude higher than the same quantities computed with δ=0 deg., therefore a thermal protection system should be needed also on the lower surface of the flap.
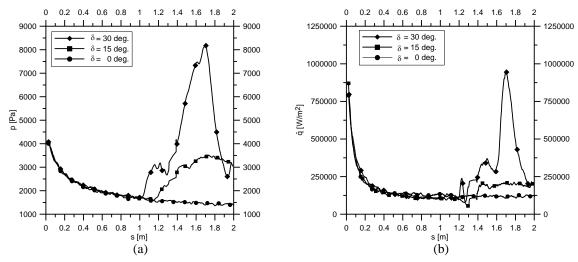
Fig. 6 Profiles of (a) pressure and (b) heat flux along the airfoil lower surface: h=65 km, α=40 deg.

Table 8 Interaction parameters: h=65 km, α=40 deg.

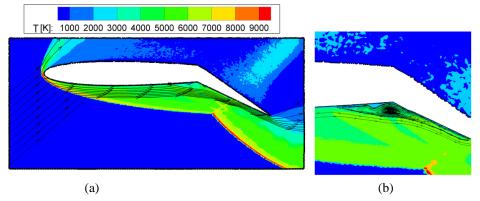| δ [deg.]	$\dot{q}_{max}/\dot{q}_{LE}$	$\dot{q}_{max}/\dot{q}_{\delta=0}$	p_{max}/p_{LE}	$p_{max}/p_{\delta=0}$
15	0.2	2.1	0.9	2.4
30	1.0	9.0	2.1	5.8

Fig. 7 (a) 2-D map of temperature and stream lines around the airfoil and (b) a zoom of region at the hinge position: h=65 km, α=40 deg., δ=30 deg.

As already said, in this case SWSWI is produced by two shock waves of the same family: one coming from the leading edge and the other one arising from the flap hinge. SWSWI produces a much stronger shock wave; the intensity of which is comparable with the one on the leading edge. As shown in Fig. 7(a), temperature behind the shock wave at the leading edge and behind the shock wave produced by interaction is about 9000 K. Stream lines are also drawn for completeness; the deflection of the stream lines, corresponding to the hinge position, is due to the shock wave from the convex angle. Fig. 7(b) shows a zoom of the picture about the hinge position; the pattern of the stream lines clearly identifies a separation bubble or "dead air" region.
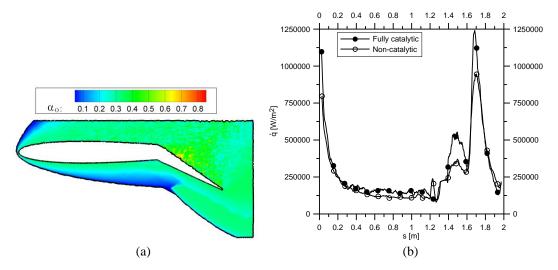
Fig. 8 (a) 2-D map of atomic Oxygen molar fraction and (b) heat flux profiles along the airfoil lower surface: h=65 km, α=40 deg., δ=30 deg.

The increase of temperature is such that air dissociation can be produced with related surface catalytic effect, increasing heat flux on airfoil surface. For example, Fig. 8(a) shows a 2-D map of the molar fraction of atomic Oxygen (α_O) produced by dissociation of molecular Oxygen. The increment of heat flux, due to the surface catalytic effect, is evidenced in Fig. 8(b) where the profiles of heat flux along the lower surface of the airfoil, with and without catalytic effects, are shown. The quantification of the catalytic effect can be provided by the two relative maxima of the profiles. The first maxima, computed considering non catalytic and fully catalytic surface, are about 3.75×10^5 and 5.50×10^5 W/m^2, the second maxima are about 1.25×10^6 and 9.38×10^5 W/m^2; the percentage increments are about 47% and 33%, respectively.

6. Conclusions

An analysis about the feasibility of an aerodynamic control by trailing edge flap deflection has been presented. The study has been carried out computationally by a direct simulation Monte Carlo code on a NACA 0010 airfoil with a flap extension of 35% of the chord. Tests have been considered in transitional regime at altitudes of 65 and 85 km, in the interval of angles of attack 0-40 deg. and with flap deflection of 0, 15, 30 deg..

The flap efficiency has been quantified by the percentage variations of aerodynamic force and longitudinal moment coefficient. The aerodynamic control, during the high altitude re-entry path, seems to be feasible and can involve fuel saving.

The shock wave-boundary layer and shock wave-shock wave interactions have been also considered. They can produce local pressure and heat flux on the flap lower surface of the same order of magnitude of those at the airfoil leading edge. This shows that a thermal protection system is necessary also on the flap lower surface.

References

Bertin, J.J. (1994), *Hypersonic Aerothermodynamics*, AIAA Education Series, Washington, USA.

Bird, G.A. (1998), *Molecular Gas Dynamics and Direct Simulation Monte Carlo*, Clarendon Press, Oxford, United Kingdom.

Bird, G.A. (2006), "Sophisticated Versus Simple DSMC", *Proceedings of the 25th International Symposium on Rarefied Gas Dynamics*, Saint Petersburg, Russia, July.

Bird, G.A. (2012), *Visual DSMC Program for Two-Dimensional Flows*, the DS2V Program User's Guide Version 4.5, Sidney, Australia.

Bird, G.A., Gallis, M.A., Torczynski, J.R. and Rader, D.J. (2009), "Accuracy and efficiency of the sophisticated direct simulation Monte Carlo algorithm for simulating non-continuum gas flows", *Phys. Fluid.*, **21**(1), DOI:10.1063/1.3067865.

BOEING X37B OBV, URL: http://www.ibtimes.com/secret-boeing-x-37b-spacecraft-finds-home-kennedy-space-center-1526688.

Delery, J. and Marvin (1986), "Shock-Wave Boundary Layer Interactions**"**, AGARD AG.280.

Delery, J. and Panaras, A. (1996), "Shock-wave boundary-layer interactions in high Mach number flows", AGARD AR-319, Vol. 1.

Edney, B.E. (1968), "Effects of Shock Impingement on Heat Transfer around Blunt Bodies", *AIAA J.*, **6**(1), 15-21.

Gallis, M.A., Torczynski, J.R., Rader, D.J. and Bird, G.A. (2009), "Convergence behavior of a new DSMC algorithm", *J. Computat. Phys.*, **228**(12), 4532-4548.

Gupta, R.N., Yos, J.M. and Thompson, R.A. (1989), "A Review of Reaction Rates and Thermodynamic Transport Properties for an 11-Species Air Model for Chemical and Thermal Non-Equilibrium Calculations to 30,000 K", NASA TM 101528.

Korkegi, R.H. (1971), "Survey of viscous interactions associated with high Mach uumber flight", *AIAA J.*, **9**(5), 771-784.

Moss, J.N. (1995), "Rarefied Flows of Planetary Entry Capsules", Special course on Capsule Aerothermodynamics, Rhode-Saint-Genèse, Belgium, May, AGARD-R-808, 95-129.

Shen, C. (2005), *Rarefied Gas Dynamic: Fundamentals, Simulations and Micro Flows*, Springer-Verlag, Berlin, Germany.

Sippel, M., van Foreest, A., Bauer, C. and Cremaschi, F. (2011), "System investigation of the SpaceLiner concept in FAST20XX", AIAA Paper, 2011-2294.

Tausche, M., Savino, R., Monti, R., Di Sotto, E., Cantos, T., Janovsky, R., Scheper, M., Apeldoorn, J., De Stefano Fumo, M., Paterna, D., Branco, J. and Molina, R. (2009), "PHOEBUS: A high lift-over-drag vehicle for Earth re-entry", *16th AIAA/DLR/DGLR International Space Planes and Hypersonic Systems and Technologies Conference*, Bremen, Germany.

Varvill R. and Bond A. (2004), "The SKYLON spaceplane", *J. British Interplan. Soc.*, **57**, 22-32.

X-51 Scramjet Engine Demonstrator-WaveRider (SED-WR), URL: http://www.globalsecurity.org/military/systems/aircraft/x-51.htm.

Zuppardi, G., Visone, G., Votta, R. and Schettino, A. (2011), "Analysis of aerodynamic performances of experimental flying test bed in high-altitude flight", *J. Aerosp. Eng.*, **225**(3), 247-258.

Zuppardi, G., Morsa, L., Sippel, M. and Schwanekamp, T. (2014), "Aero-thermo-dynamic analysis of the SpaceLiner-7.1 vehicle in high altitude flight", *Proceedings of the 29th International Symposium on Rarefied Gas Dynamics*, Xian (China), July.

EC